Proceedings of the 32nd Chinese Control Conference
July 26-28, 2013, Xi'an, China

Autonomous Takeoff, Tracking and Landing of a UAV on a Moving UGV Using Onboard Monocular Vision

Cheng Hui[1], Chen Yousheng[1], Li Xiaokun[1], Wong Wing Shing[2]

1. Dept. of Automation, Sun Yat-sen University, Guangzhou, China
E-mail: chengh9@mail.sysu.edu.cn

2. Dept. of Information Engineering, The Chinese University of Hong Kong, Hong Kong
E-mail: wswong@ie.cuhk.edu.hk

Abstract: In this paper, we present a monocular vision based approach for cooperation between a micro unmanned aerial vehicle (UAV) and an unmanned ground vehicle (UGV). By tracking the target marker on the UGV, the UAV can autonomously track and land on the moving UGV. Closed control loops based on PID controllers are employed to accomplish two levels of control: low-level self-stabilized flight control, and high-level position control. The self-stabilized flight control is executed on an onboard microcontroller board with the aid of a 9-DOF inertial measurement unit (IMU). The images captured by the onboard low-cost camera are transmitted to the land laptop over wireless channels. The relative position of the UAV to the ground moving vehicle is estimated from the received images via a land laptop. The estimated current position is sent to the UAV via wireless channels. The proposed visual-based approach to detect and locate the target marker is robust to cluttered ground background as well as the height of the UAV. Practical experiments show that the UAV can autonomously track the moving UGV, and autonomously land on the landing marker on the moving UGV.

Key Words: UAV, UGV, quadrotor, monocular vision, IMU, hovering, tracking, landing

1 Introduction

Autonomous flight of a micro Unmanned Aerial Vehicle (UAV) has attracted much research efforts during the past few years. Autonomous flight of UAV is demanded in applications in surveillance, rescue and aerial observation. Vision-based autonomous hovering and landing is vital for autonomous flight in GPS-denied environments.

Currently, research on vision-based location and tracking during flights has been mainly for helicopter with large dimension and high mass [1] [2]. With the development of high-efficiency brushless DC motors and high-capacity batteries, UAVs become lighter and smaller, and can achieve longer flight time for new applications. In [3], S. W. Yang et al. presented an onboard vision system to detect the landing pad, where the 5 degrees of freedom (DOF) pose of the UAV is estimated via an onboard camera. In [4], S. Lange et al. proposed an efficient design of the landing marker as well as a vision-based landing marker detection algorithm. In [5], a dual camera is adopted to estimate the 6-DOF pose of the UAV. Location is achieved via an onboard camera and a camera on the ground. L. Meier et al. [6] developed a UAV system using an inertial measurement unit (IMU) and four onboard cameras for purposes of localization, pattern recognition and obstacle avoidance. K. E. Wenzel et al. [7] presented visual autonomous hovering in a defined position using a Wii infrared camera to track infrared spots at the landing target. As UAVs are highly agile, it is not sufficient to perform pose control directly using visual pose estimation as low-frequent vision updates. In addition, approaches using multiple cameras with complex detection algorithms require expensive image-processing computations.

The UAVs offer a broad field of view and a complete 3-D sensing at higher speed compared with ground vehicles. However, the payload of micro UAVs is very limited. On the contrary, unmanned ground vehicles (UGVs) offer high-resolution views over short ranges, high payload and longer running time, although they have limited field of view and low coverage speed. The coordination between groups of UAVs and UGVs is of interests in reconnaissance and exploration applications [8] [9]. Cooperative air and ground surveillance strategies are presented in [10] for high mass fixed-wing UAVs with the aid of GPS and onboard cameras. In [11], a vision-based approach was presented for UAVs achieving autonomous tracking and landing on a moving carrier via an onboard infrared camera and ground infrared LED sources. Tracking of IR LEDs can be hindered by sunlight [11], and the sensing range is limited. In [12], stable tracking and safe landing of an UAV on an UGV was presented, where the UGV moved at velocities of 0.1 and 0.3 m/s, and two LED markers on the UGV were employed as the flight guidance for the UAV.

In the paper, a visual-based approach employing a single onboard camera is presented for cooperation between an UAV and an UGV. The proposed visual-based approach is more flexible for UAVs to detect and track various objects compared with the schemes in [11] [12] employing LEDs for the flight guidance. Our platform consists of a quadrotor UAV and a holonomic UGV. A circle-shaped marker on the UGV is used as the landing marker. A low-cost camera on the UAV is employed to detect the target circle. By tracking the marker, the UAV achieves autonomous tracking and landing on the UGV. The sensor data of a 9-DOF IMU are fused to estimate attitude of the UAV. As the UAV is highly nonlinear, its accurate dynamical model is challenging to obtain. Standard PID controllers are used to accomplish self-stabilized fights. Moreover, closed-loop PID position controls executed on the UAV's onboard microcontroller achieve autonomous tracking and landing on the UGV.

The paper is organized as follows. In Section II, the UAV and the UGV platforms are described. The self-stabilization

*This work is supported by project MMT-p3-11 of the Shun Hing Institute of Advanced Engineering, CUHK, and National Natural Science Foundation of China under Grants 60804012 and 61174060, and Shenzhen matching grant GJHS20120702105523301.

control of the UAV is also addressed. Section III presents a vision-based approach for cooperation between the UAV and the UGV. In Section IV, experimental results are presented and analyzed. Section V concludes the paper.

2 System Description and Self-stabilized Flight

In this section, we give a description of our platform consisting of a micro quadrotor and a holonomic mobile robot, as shown in Fig. 1.

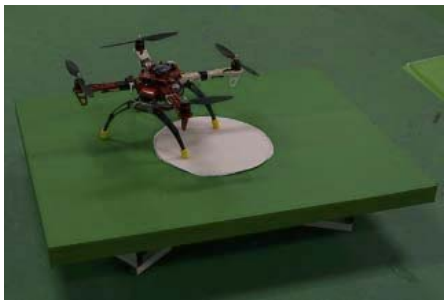

Fig. 1. The platform consists of a quadrotor and a vehicle.

- ***The quadrotor UAV platform***

The quadrotor UAV platform is shown in Fig. 2. The quadrotor model is DJI F450, which weights 1.2 kg with a payload capability up to 0.3 kg, and spans a diameter of 0.5 m. The quadrotor is propelled by four brushless DC motors, and can move in 6-DOF by varying speeds of the four rotors. Onboard sensors consist of a 9-DOF IMU, a sonar sensor, and a downward-looking camera. A monocular camera of 40 g weight is mounted at the geometric center of the UAV, with a maximum frame rate of 25 fps, and a lens with view angle of approximately 85^0. A 9-DOF IMU is applied to estimating the current attitude position of the UAV. The sonar sensor is used to measure the flight height.

An onboard microcontroller board based on a 100 MHz ARM Cortex-M4 processor achieves UAV autonomous stabilization flight. The relative position of the UAV to the moving UGV is estimated from received images. The UAV communicates with the ground station via two wireless radio frequency modules. The ground station is a laptop with an Intel®Core™ i7-3610QM 2.3 GHz processor, which sends the estimated relative position of the UAV to the ground vehicle, remotely adjusts the working parameters, displays real-time UAV status, as well as initiates departure and landing of the UAV. A landing marker with a radius of 20 cm is circle- shaped, as shown in Fig. 2.

Fig. 2. The quadrotor platform and the landing marker.

- ***The UGV platform***

A three-wheeled vehicle platform of $82\times63\times14$ cm with

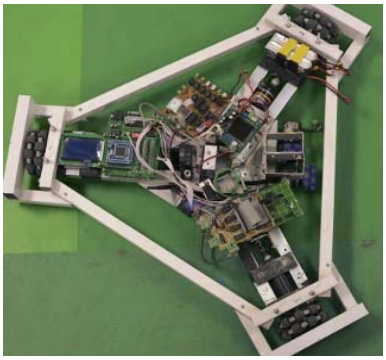

Fig. 3. A three-wheeled vehicle with omnidirectional wheels is designed as the ground vehicle.

omnidirectional wheels was designed as the UGV, as shown in Fig. 3. The velocity of the UGV is measured by three incremental optical encoders with 500 pulses/rev. The onboard microcontroller for velocity and position control is based on a 40 MHz 16 bit Freescale MC9S12XS128 processor. Sensor information is transmitted to the ground station via a ZigBee module. The ground station monitors real-time UGV status, alters controlling parameters, as well as sets the desired velocities and trajectories. A plank of $103\times80\times6$ cm covered on the UGV was used as the landing pad. By tracking the circle-shaped landing marker attached on the landing pad, the UAV executes autonomous tracking and landing on the UGV.

Without considering the air resistance and the self-caused air turbulences, the dynamical model of the quadrotor can be represented as [13]:

$$\begin{cases} \ddot{x} = (\cos\psi\sin\theta\cos\phi + \sin\psi\sin\phi)U_1 / m \\ \ddot{y} = (\sin\psi\sin\theta\cos\phi - \cos\psi\sin\phi)U_1 / m \\ \ddot{z} = (\cos\theta\cos\phi)U_1 / m - \mathrm{g} \\ \ddot{\phi} = l(U_2 + \dot{\theta}\dot{\psi}(I_y - I_z)) / I_x \\ \ddot{\theta} = l(U_3 + \dot{\phi}\dot{\psi}(I_z - I_x)) / I_y \\ \ddot{\psi} = (U_4 + \dot{\phi}\dot{\theta}(I_x - I_y)) / I_z \end{cases} \quad (1)$$

where (x, y, z) is the linear position defined in the inertial frame, the attitude vector (ϕ, θ, φ) defined in the inertial frame denote the roll, pitch and yaw respectively, (I_x, I_y, I_z) are the moments of the inertia with respect to the axes, U_1 is the vertical thrust, (U_2, U_3, U_4) represent the rolling, pitching and yawing moments respectively, g is gravitational acceleration, and l is the distance between the rotor and the center of the mass of the quadrotor.

The dynamics of the quadrotor is highly nonlinear, and the control of its attitude is coupling. When the quadrotor is hovering, the angles (ϕ, θ, φ) are approaching to zeros. The nonlinear dynamics hence can be linearized, and the 6-DOF pose of the UAV can be independently controlled. With the linearization and the decoupling, autonomous stabilization flights are achieved by three independent PID controllers.

In the paper, the attitude of a UAV is estimated using a 9-DOF IMU, which combines a tri-axis gyroscope, a tri-axis accelerometer and a tri-axis magnetometer. Gyros can measure relative angular rates with the disadvantage of gyro drift. Accelerometers and magnetometers data are used to compensate gyroscope measurement errors. An orientation

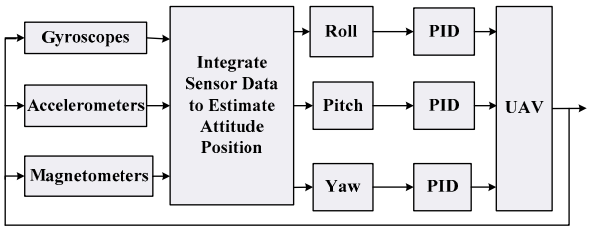

Fig. 4. Control structure for autonomous stabilization flight.

estimate algorithm using a quaternion representation was proposed in [14] to efficiently fuse separate sensor data of IMUs for rehabilitation applications. It was shown that the performance of the algorithm achieves levels of accuracy matching that of conventional Kalman-based algorithms with low computational load. By virtue of the orientation estimate algorithm [14], the measured data of the IMUs are fused to provide a complete attitude estimation of the UAV. Transforming the quaternion representation to Euler angles [15], the attitude of the UAV can be obtained as follows:

$$\begin{aligned}
&\theta = \arcsin(2q_2q_3 + 2q_0q_1),\ \theta \in (-\pi/2, \pi/2),\\
&\phi = \arctan\frac{-2(q_1q_3 - q_0q_2)}{q_0^2 - q_1^2 - q_2^2 + q_3^2},\ \phi \in (-\pi/2, \pi/2),\\
&\psi = \arctan\frac{-2(q_1q_2 - q_0q_3)}{q_0^2 - q_1^2 + q_2^2 - q_3^2},\ \psi \in (-\pi, \pi),
\end{aligned} \tag{2}$$

where the vector (q_0, q_1, q_2, q_3) denotes four basic elements of a quaternion q. The current quaternion can be iteratively estimated by the optimized gradient descent algorithm [14].

Fig. 4 illustrates the control structure for autonomous stabilization flights. The attitude estimation and the control algorithms are executed on an onboard microcontroller based on an ARM Cortex-M4 processor in real-time.

3 Autonomous Takeoff, Tracking & Landing of UAVs using an On-board Monocular Camera

In this section, a visual-based approach is proposed for UAVs to accomplish autonomous taking off, tracking and landing on a UGV. As absolute linear positions (x, y, z) can not be obtained from the onboard IMU, visual based navigation is critical for autonomous flights in GPS-denied environments. A low-cost monocular camera is mounted at the geometric center of the UAV downwards. A circle with a radius of 20 cm attached on the landing pad of the ground vehicle is used as a landing marker. The relative position of the target circle can be estimated with the aid of an onboard camera. The images captured by the onboard camera are transmitted to the land laptop over wireless channels. The laptop detects the target marker from the received image, estimates the currently relative position to the center of the target circle, and transmits the estimated relative position over a wireless radio frequency transmission module.

3.1 Vision based target position estimate

The image transmitted over wireless channels will be dropped and contaminated by noise. In the following, the process of vision-based feature extraction from the noisy images is addressed. Pre-processing steps are employed to mitigate noise and improve the effects of feature extraction. Fig. 5 shows the vision-based detection process.

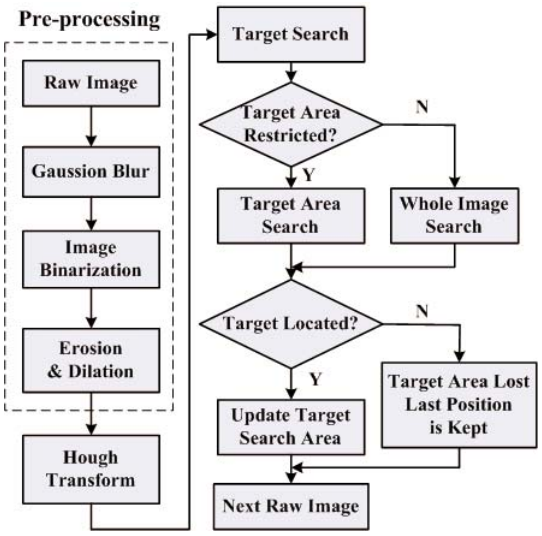

Fig. 5. The vision-based architecture.

- ***Gaussian Smoothing***

Gaussian blur is used to obtain a smooth digital image. The equation of a discrete Gaussian function with zero mean in two dimensions is:

$$g[i, j] = e^{\frac{-(i^2 - j^2)}{2\sigma^2}}, \tag{3}$$

where $g[i, j]$ denotes the (i, j)-th element of a matrix, and σ is the standard deviation related to the smoothing effect.

Using the Gaussian blur's separable property, the Gaussian blur process in two dimensions can be divided into two independent one-dimensional passes. Considering a 640×480 image, a matrix with dimensions $[3, 3]$ is calculated with $\sigma = 1$. After Gaussian smoothing, the RGB image is transformed to grayscale image.

- ***Adaptive thresholding***

In flights, especially during vertical takeoff and landing, the light intensity varies dramatically. To reduce adverse effects of light intensity, the classical Otsu method is used to perform adaptive thresholding. A binary image is hence obtained from a grayscale image.

- ***Erosion and dilation***

The erosion operation aims to erode away the boundaries of regions of foreground pixels. While the dilation operator gradually enlarges the boundaries of regions of foreground pixels, thus areas of foreground pixels grow in size. Opening operation performed on a binary image is the dilation of the eroded image. A 5×5 square structuring element is used to provide erosion and expansion effects. To remove the isolated pixels in the eroded image, a two-dimensional median filter is applied:

$$g(x, y) = median\{f(x - k), y - l\}, \quad k, l \in W \tag{4}$$

where $f(x, y)$ and $g(x, y)$ are the original/filtered image respectively, and a 5×5 rectangular window W is used.

- ***Target circle search***

A noiseless binary image can be obtained by performing the pre-processing steps mentioned above. Hough transformation is employed to detect the target circle, which is used as the landing marker. Since the area of the target circle is

specified, a circle with an area within an appropriate range can be identified as the target circle:

$$S_{\min} < S < S_{\max}, \quad (5)$$

where S is the currently calculated search area; $S_{\min}$ and $S_{\max}$ denote the minimum and maximum circle area.

The search area on the sequential image will be restricted within a square when the target circle is located. Through conforming the center of the square to that of the target circle, the side of the square is set to the diameter of the target circle plus a constant. With the aid of the restricted search area, the computational load of the target location algorithm can be highly decreased. Moreover, the detection approach is robust to interference outside the restricted search area. When the target area is lost, target search is performed over the whole image instead of only searching within the restricted area. If a unique circle is identified on the search area, it is assumed to be the target circle. On the other hand, if more circles appear, the circle, whose center position is nearest to that of the latest identified target circle, is updated as the target circle. In flight experiments, it is shown that the target circle can be successfully identified and located if it is not lost during initial target searching.

Fig. 6 (a) shows the original image of the onboard camera, where the right circle is the landing marker, while the left one is added as a disturbance. Meanwhile, Fig. 6 (b) shows the processed and detected images. In Fig. 6 (b), the square denotes the restricted target search area, the circle within the square is the target circle, and the smallest circle within the square represents the center of the target circle. Using the scheme to restrict the target search area within a square, as shown in Fig. 6 (b), the target circle can be successfully identified even with a interfered circle is added in the image. Moreover, experiments showed that the target circle can be successfully detected in cluttered environments.

The proposed visual-based landing marker detection approach executed in the laptop costs only about 25~30 ms to complete the calculations. The laptop can be carried by the cooperating UGV. Moreover, it is promising for UAVs to perform the proposed vision-based approach on an onboard microcontroller. The estimated relative position of the target circle's center is sent to the UAV via a wireless radio frequency module. Therefore, the UAV automatically adjusts its current position (x, y) according to the position errors via closed-loop PID controllers.

3.2 Autonomous hovering, tracking and landing

A sonar sensor is used to measure the altitude of the UAV. In order to mitigate adverse effects of high frequency vibrations of the UAV, the contaminated data of the sonar

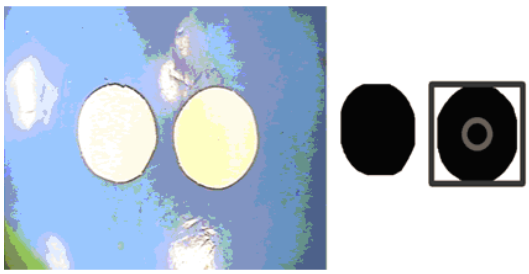

(a) (b)

Fig. 6. (a) The aerial live view; (b) the detected objects using pre-processing steps and circle detection.

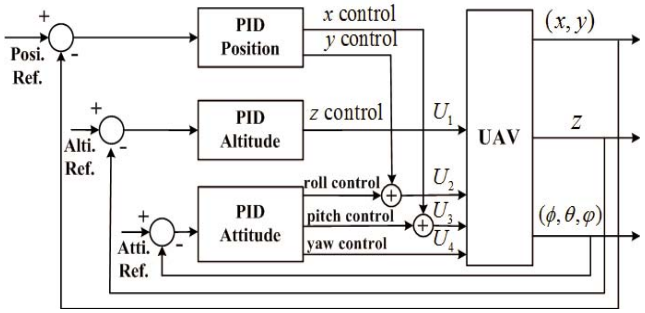

Fig. 7. Control architecture for autonomous hovering and tracking.

sensor is smoothed by a median filter with a window of 9. A standard PID controller is applied to keep the specified altitude of the UAV. With the feedback relative position, closed-loop PID position controllers are employed to achieve autonomous hovering. Similarly, when the UGV with the landing marker moves, the UAV autonomously tracks the moving vehicle.

Fig. 7 shows the control diagram for autonomous takeoff, hovering and tracking with six independent closed-loop PID controllers with three inner-loop controls realizing self-stabilized flight and three outer-loop controls for position controls. The altitude controller output is used as the vertical thrust U_1; the yaw controller output is related to the yawing moment U_4; the rolling moment U_2 is acquired by adding the outputs of the x position and the roll controllers; and the pitching moment U_3 is obtained by summing the outputs of the y position and the pitch controllers.

4 Experimental Flights

The proposed vision-based approach for cooperation between a UAV and a UGV has been performed on the platforms. Extensive experiments were performed to obtain accurate controlling parameters for PID controllers and other working parameters. Plenty of flights have proven that the UAV platform has good controlling abilities. By tracking the landing marker on the ground vehicle, various experiments demonstrated that the UAV can autonomously track and land on the moving vehicle. Fig. 8 shows the schematic architecture of the UAV platform. The control frequency for low-level stabilization flight control is 400Hz, which is much higher than those for the high-level position control. Images transmitted over wireless channels are noisy and may be lost, which leads to the outliers of position errors. To remove the outliers of position errors, the latest effective position estimate is used when the current absolute position error in x or y is larger than 20 cm. The ground station graphical user interface depicted in Fig. 9 illustrates the aerial live view and the detected landing marker.

Various scenarios were examined. In the first scenario, the UAV autonomously hovers at a set point. In the second scenario, the UGV moved at constant or varying velocities, where the UGV moved in circular paths or tortuous paths with sharp turns.

A demo video can be found online at [16].

4.1 Autonomous vertical takeoff, landing and hovering at a set point

In the experiments, the UAV accomplished autonomous

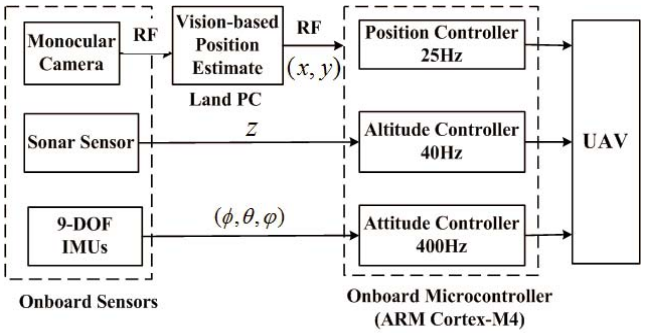

Fig. 8. Schematic architecture of the UAV platform.

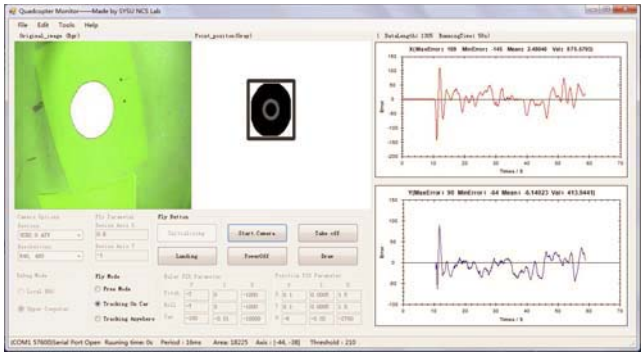

Fig. 9. The live view and the detected landing marker shown in the ground station graphical user interface.

vertical takeoff, landing, as well as hovering at a set point of $(0,0,120)$. Fig. 10 depicts the real-time angular and linear positions of the UAV. It can be seen from Fig. 10 (a) that the angular positions have relatively larger jitters due to the ground effect of the UAV during the vertical takeoff phase. When the flight height exceeds 0.28 m, the self-stabilized flight is achieved with the fading of the ground effect, and the angular positions are kept within ± 2 degrees. The UAV autonomously hovers when it reaches the specified height. Similarly to the takeoff phase, during the vertical landing at about 100 seconds, the angular positions have relatively larger fluctuations. Fig. 10 (b) shows the measured positions in x, y and z. As shown in Fig. 10 (b), the measured altitude of the UAV is close to the desired height of 120 cm. It can be seen that relatively larger position errors in x and y occur during takeoff and landing phases. It is because the UAV is relatively unstable during initial takeoff, in addition, the visual-based position estimate is unavailable when the flight height is lower than about 0.28 m.

The control performance of the UAV in the presence of external perturbations was investigated. Fig. 11 presents the angular and linear positions of the UAV under perturbations when hovering at a set point of $(0,0,140)$. Impulse forces were executed to the UAV in y and x axes at around 21 and 31 seconds respectively, resulting in relatively larger position errors in x and y. As shown in Fig. 11 (b), the positions in x and y immediately retrieved to the desired position with the PID position controllers. Accordingly, the roll ϕ and pitch θ instantly altered to realize stabilization flight. Experiments demonstrated that the self-stabilized flight control is robust to external perturbations.

4.2 Autonomous taking off, tracking and landing on a moving UGV

In the experimental flights, the UAV autonomously track and land on the UGV by tracking the landing marker on the moving UGV. The UGV moved in a circular path with a diameter of 2 m at a constant velocity of 0.63 m/s. Fig. 12 shows the control performance of the UAV in one autonomous flight. Fig. 12 (b) shows the measured positions in x, y and z. As shown in Fig. 12 (b), the position errors in x and y are within about ± 20 cm, illustrating that the UAV can well track and land on the moving UGV via the presented vision-based approach.

The cases of the UGV moving in tortuous paths with sharp turns were also examined. The UGV turned sharply at 90^0 clockwise and counterclockwise in x and y axes at velocities varying from 1 m/s to 1.2 m/s. Fig. 13 shows the tracking performance in such cases. Fig. 13 (b) illustrates the actual positions in x, y and z. Experimental results show that the UAV can well track and land on the UGV moving at sharp turns. Compared to the position errors as the UGV moved in smooth paths at lower velocities, it can be seen that larger angle and position errors were introduced as the UGV moved in tortuous paths. Especially, relatively larger position errors occur at the turning corners.

Autonomous landing of the UAV on the landing target is challenging, especially when landing on the moving UGV. When the UGV moves in smooth paths at velocities less than 1.2 m/s, the successful rate of 88.24% was achieved for the UAV autonomously landing on the target circle on the UGV in a sequence of seventeen autonomous flights. A higher successful rate of 93.75% was achieved for the UAV autonomously landing on the target circle on the stationary UGV in a sequence of sixteen flights.

Considering fifteen successfully autonomous flights for vertically takeoff, landing and hovering at a set point, Table 1 presents the control performance with respect to the mean, standard deviation and maximum absolute value of angle and position errors. Meanwhile, Table 2 shows the control performance of fifteen successfully autonomous flights for the UAV takeoff, tracking and landing on the UGV, where the UGV moved on circular paths at a constant velocity of 0.67 m/s. Since the vision-based position estimate is unavailable when the camera is close to the landing target, the position errors in x and y were calculated as the flight height is larger than a threshold of 0.28 m. It can be shown from Tables 1 and 2 that the angle and position errors of the UAV tracking the moving UGV are larger than those of the UAV hovering at a set point. Table 3 shows the position errors in x and y at the landing point in fifteen successfully autonomous flights considering two cases that the UGV is stationary or moving in circular paths. As shown in Table 3, the maximum absolute position errors in x and y are less than the radius of 20 cm of the target circle. It illustrates that the UAV can autonomously land on the target circle on the stationary or moving UGV.

Currently, the positions in x and y were estimated from images of resolution 640×480 at the height of 120 or 140 cm. More accurate position estimation in x and y can be achieved with higher image resolution.

Table 1: Control performance of 15 successfully flights with UAV autonomously takeoff, landing and hovering at a set point

	x(cm)	y(cm)	ϕ(deg)	θ(deg)	φ(deg)
Mean	-0.8536	-3.1479	-0.1690	-0.0915	0.4615
Standard deviation	4.8007	5.5799	0.6314	0.5648	0.4933
Max. abs. error	26.5607	33.4787	3.4625	4.1367	1.6982

Table 2: Control performance of 15 successfully flights with UAV autonomously tracking and landing on a moving UGV

	x(cm)	y(cm)	ϕ(deg)	θ(deg)	φ(deg)
Mean	-1.5693	-1.8940	-0.8382	-0.0947	0.6260
Standard deviation	6.0005	6.3877	0.7750	0.7255	0.4355
Max. abs. error	32.8467	42.9473	4.7791	5.3022	1.7746

Table 3: Position errors at the landing point for 15 successfully autonomous flights as the UGV stationary or moving

	Mean	Standard deviation	Max. abs. error
x, y (cm) (stationary UGV)	0.4813/0.3278	4.8007/5.0371	7.8000/13.2480
x, y (cm) (moving UGV)	5.7989/3.4395	5.5799/9.2179	15.800/16.0752

5 Conclusions

In this paper, we presented a visual-based approach to achieve cooperation between a UAV and a UGV using a single onboard camera. The UAV can autonomously track and land on the moving UGV by detecting the target circle on the UGV. Closed control loops based on PID controllers, executed on an onboard microcontroller board on the UAV, were employed to achieve 6-DOF pose controls. Through fusing the measured data from a 9-DOF IMU, the attitude of the UAV was estimated to accomplish self-stabilized flights. From noisy images captured by the onboard camera, the relative position of the UAV to the UGV can be estimated via a land laptop. The laptop can be carried by the cooperating UGV. It is also promising for UAVs to perform object detection on an onboard microcontroller since the proposed visual-based approach is computationally efficient. The proposed vision-based approach provides a flexible criterion to detect and track various objects. Practical experiments show that the UAV can successfully achieve autonomous taking off, tracking and landing on the moving UGV via the proposed vision-based approach.

In future work, faster and smoother tacking of moving UGV for UAVs will be investigated. Velocity control via optical flow techniques will be examined. Wide-angle lens or pan-tilt cameras will be considered to obtain broader field of view in order to detect and track faster moving object. In addition, to improve the estimation accuracy of relative position, images with higher resolution will be acquired, demanding more efficient image processing algorithms. It is of interests to study cooperation among multiple UAVs and UGVs through simulations and experiments.

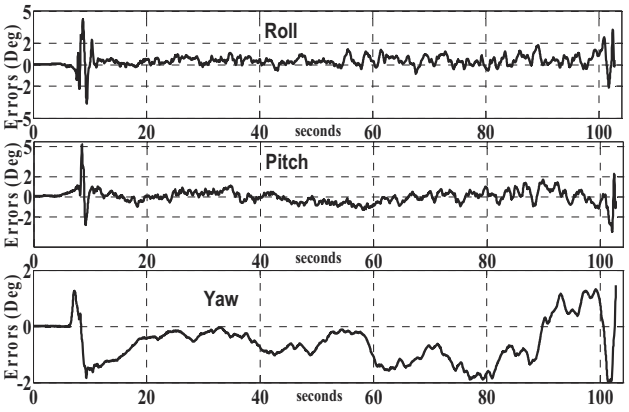

(a) Measured angles (ϕ, θ, φ) of the UAV.

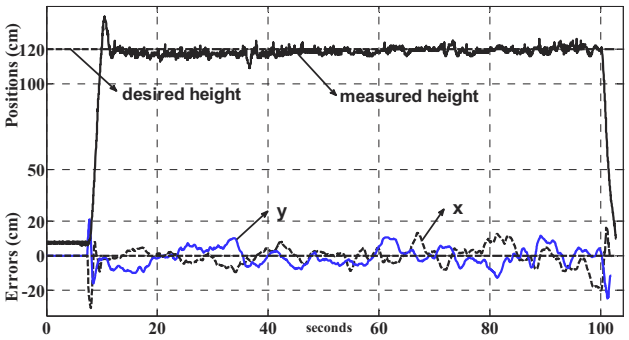

(b) Measured positions (x, y, z) of the UAV.

Fig. 10. Autonomous takeoff, hovering and landing of the UAV. (a) Measured angles in degrees. (b) Measured translational positions.

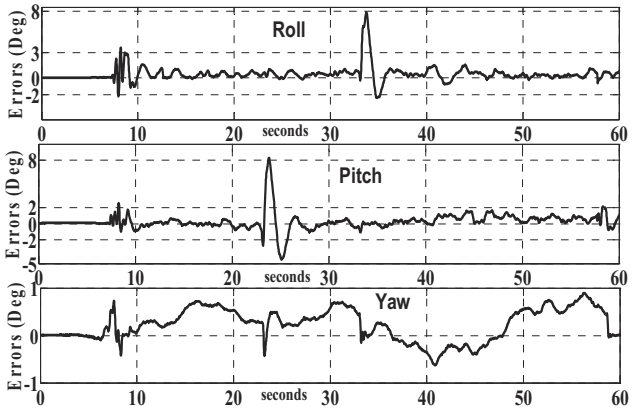

(a) Measured angles (ϕ, θ, φ) of the UAV.

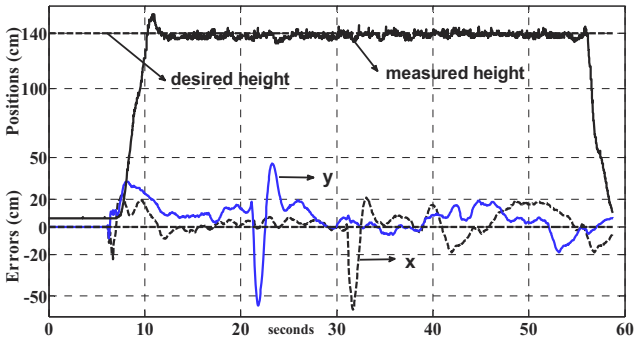

(b) Measured positions (x, y, z) of the UAV.

Fig. 11. Autonomous takeoff, hovering and landing of the UAV under external perturbations. (a) Measured angles in degrees. (b) Measured translational position.

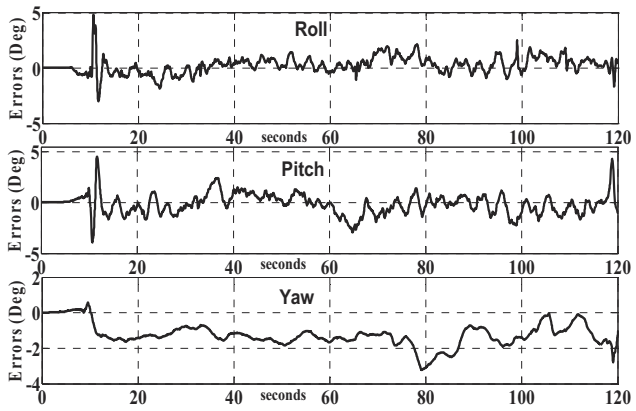

(a) Measured angles (ϕ,θ,φ) of the UAV.

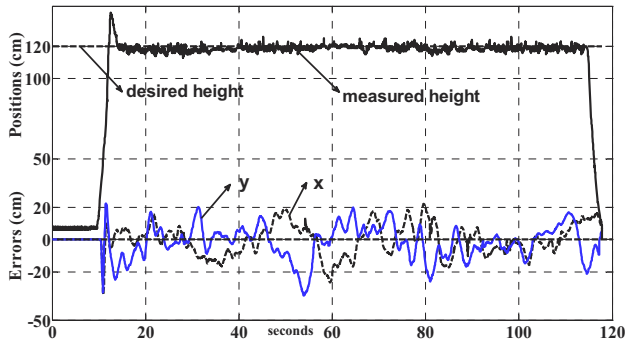

(b) Measured positions (x,y,z) of the UAV.

Fig. 12. Autonomous takeoff, hovering and landing of the UAV as the ground vehicle moves in circular paths. (a) Measured angles in degrees. (b) Measured translational position.

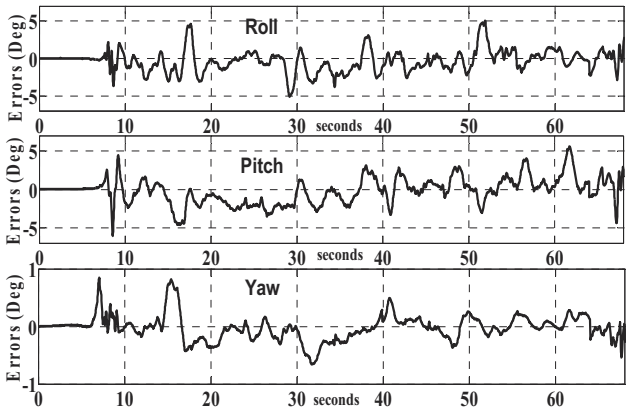

(a) Measured angles (ϕ,θ,φ) of the UAV.

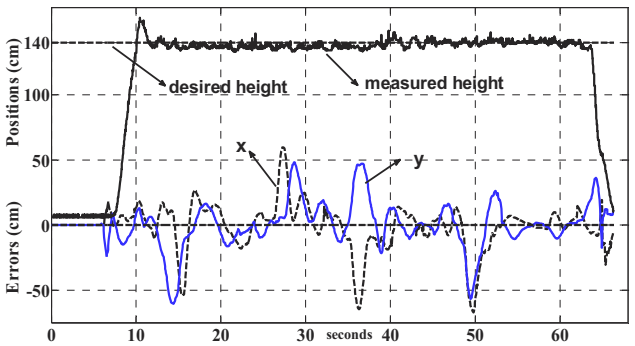

(b) Measured positions (x,y,z) of the UAV.

Fig. 13. Autonomous takeoff, hovering and landing of the UAV as the ground vehicle moves in tortuous paths with sharp turns. (a) Measured angles in degrees. (b) Measured translational positions.

Acknowledgements

The authors would like to thank Mr. Huang Z. J. for the printed circuit board layout of the onboard microcontroller board for the UAV platform.

References

[1] Klas Nordberg, Patrick Doherty, et al., Vision for a UAV helicopter, *Proc. of IROS Workshop on Aerial Robotics*, pp. 1-6, Lausanne, 2002.

[2] Mcgee T., Zuwhan Kim, Xiao X. et al., Vision-based road-following using a small autonomous aircraft, *Proc. of IEEE Conf. Aerospace*, pp. 3006–3015, Montana, Mar. 2004.

[3] S. W. Yang, S. A. Scherer and A. Zell, An onboard monocular vision system for autonomous takeoff, hovering and landing of a micro aerial vehicle, *J. Intell. Robot Syst.*, Sep. 2012, Springer, published online.

[4] S. Lange, N. Sunderhauf, P. Protzel, A vision based onboard approach for landing and position control of an autonomous multirotor UAV in GPS-denied environments, *Proc. of Conf. on Advanced Robotics*, pp. 1-6, Munich, June 2009.

[5] Ly Dat Minh, Cheolkeun Ha, Modeling and control of quadrotor UAV using vision-based measurement, *Proc. of Int. Forum on Strategic Technology*, pp.70-75, Ulsan, Oct. 2010.

[6] L. Meier, P. Tanskanen, F. Fraundorfer, M. Pollefeys, PIXHAWK: A system for autonomous flight using onboard computer vision, *Proc. of IEEE Conf. Robotics & Automation*, pp. 2992-2997, Shanghai, May 2011.

[7] K. E. Wenzel, P. Rosset, A. Zell, Low-cost visual tracking of a landing place and hovering flight control with a microcontroller, *J. Intell. Robot Syst.*, 57(1): 297-311, 2010.

[8] L. Chaimowicz and V. Kumar, Aerial shepherds: coordination among UAVs and swarms of robots, *Proc. of Int. Symp. Distributed Autonomous Robotic Systems*, Toulouse, pp. 243-252, June 2004.

[9] N. Michael, J. Fink and V. Kumar, Controlling a team of ground robots via an aerial robot, *Proc. of Int. Conf. Intelligent Robots and Systems*, pp. 965-970, San Diego, CA, Oct. 2007.

[10] B. Grocholsky, J. keller, V. Kumar and G. Pappas, Cooperative air and ground surveillance, *IEEE Robotics & Automation Magazine*, 13(3):16- 25, Sep. 2006.

[11] K. E. Wenzel, A. Masselli and A. Zell, Automatic take off, tracking and landing of a miniature UAV on a moving carrier vehicle, *J. Intell. Robot Syst.*, 61(1): 221-238, Jan. 2011.

[12] W. Li, T. G. Zhang *and* Kolja Kuhnlenz, A vision-guided autonomous quadrotor in an air-ground multi-robot system, *Proc. of IEEE Conf. Robotics & Automation*, pp. 2980-2985, Shanghai, May 2011.

[13] A. L. Salih, M. Moghavvemi et al., Modelling and PID controller design for a quadrotor unmanned air vehicle, *Proc. of IEEE Conf. Automation Quality and Testing Robotics*, pp.1-5, Romania, May 2010.

[14] Sebastian O.H. Madgwick, Andrew J.L. Harrison, Ravi Vaidyanathan, Estimation of IMU and MARG orientation using a gradient descent algorithm, *Proc. of IEEE Conf. Rehabilitation Robotics*, pp. 1-7, Zurich, June 2011.

[15] Ken Shoemake, Animating rotation with quaternion curves, *Proc. of 12th SIGGRAPH*, pp. 245-254, San Francisco, July 1985.

[16] Demo video online available at the project website: http://personal.ie.cuhk.edu.hk/~wswong/project%20webpage/Quadcopterandlanding.avi